Surface effect on the electrical and optical properties of barium titanate at room temperature

H. Chaib, L. M. Eng,* F. Schlaphof, and T. Otto
Institute of Applied Photophysics, University of Technology Dresden, D-01062 Dresden, Germany
(Received 23 April 2004; revised manuscript received 24 September 2004; published 25 February 2005)

The surface effect on the electrical and optical properties of tetragonal barium titanate at room temperature is investigated theoretically by using a microscopic model based on the orbital approximation in correlation with the dipole–dipole interaction. Both the first-, second-, and third-order electronic polarizabilities were considered in this calculation in order to obtain accurate results for both the spontaneous polarization and refractive indices. All types of surfaces were studied, either being *a*- or $c^{\pm}$-surfaces (both BaO- and TiO_2-terminated). The spontaneous polarization is drastically reduced near the *c*-surfaces while it remains almost unchanged near the *a*-surfaces. Furthermore, both the *a*- and $c^{\pm}$-surfaces show the tendency to deeply reduce the refractive index for light polarized perpendicular to the surface.

DOI: 10.1103/PhysRevB.71.085418 PACS number(s): 78.20.Bh, 78.20.Ci, 77.22.Ej, 77.84.Dy

I. INTRODUCTION

Tetragonal barium titanate ($BaTiO_3$) is a ferroelectric oxide material of enormous importance for potential applications that make use of its unusual piezoelectric, ferroelectric, dielectric, optic, electro-optic, and photorefractive properties. Many of these applications are increasingly oriented toward thin films geometries, where surface/interface properties are of growing importance.[1–6]

Here we present a quantum mechanical theoretical approach for studying the spontaneous polarization, refractive indices, and polarization properties of $BaTiO_3$ at the surface of *a*- and *c*-domains at room temperature. The latter are either BaO or TiO_2 terminated. Our microscopic model takes into account the anisotropy in the first-, second-, and third-order electronic polarizabilities of all constituent ions, their ionic shifts as well as the crystalline deformations. The model was previously tested for the calculation of bulk properties of monodomain tetragonal perovskites like tetragonal $BaTiO_3$ and $KNbO_3$, i.e., their ferroelectricity and optical anisotropy as well as their linear electro-optical coefficients.[7–9] Furthermore the same model was successfully applied for modeling electrical and optical properties of rhombohedral $LiNbO_3$ single crystals,[10] as well as 90 and 180° ferroelectric domain walls in $BaTiO_3$.[11]

Based on those experiences, which agree very well with the corresponding experimental data, we initiate the application of this model to $BaTiO_3$ surfaces in tetragonal phase. Such an investigation is of great help in comparing experimental and theoretical findings.

In this model, we account for the following points:

- Expansion of the local electric field by simultaneously considering its components in all directions;
- representation of the local electric field in a tensorial equation allowing the description of all field components for all ions simultaneously;
- development of the orbital approximation by taking into account the anisotropy in the first-, second-, and third-order electronic polarizabilities of the constituent ions;
- consideration of the correlation between the first-, second-, and third-order electronic polarizabilities on one hand, and their dependence on the local electric field on the other hand (since these magnitudes are mutually dependent).

The paper is structured as follows: Section II briefly discusses the first-, second-, and third-order electronic polarizabilities of constituent ions in tetragonal $BaTiO_3$ by using the quantum mechanical method based on the orbital approximation. Next we discuss the dipole–dipole interaction due to the local electric field acting on the constituent ions taking into account the crystalline deformations and individual ionic shifts near the sample surface. Section III then presents the results for the spontaneous polarization, as well as the refractive indices calculated for tetragonal $BaTiO_3$ surfaces at room temperature. This section also contains the discussion of the above-mentioned findings.

II. DESCRIPTION OF THE MODEL

A. Orbital approximation

In order to compute the first-, second-, and third-order electronic polarizabilities of $BaTiO_3$, we use a quantum mechanical approach based upon the orbital approximation. In this approach, each ion is considered as the core consisting of all inner electrons and the nucleus, while the shell carries the outer electron. The Hamiltonian of this core-shell system is written as

$$H = H_0 + H_1, \tag{1}$$

with

$$H_0 = \frac{p^2}{2m} - \frac{Z^{*\mathrm{n}}}{R}e^2, \tag{2}$$

$$H_1 = e\mathbf{E}\cdot\mathbf{R}, \tag{3}$$

where H_0 represents the Hamiltonian in absence of the local electric field, and H_1 describes the perturbation due to the local electric field. In Eqs. (2) and (3) $Z^{*\mathrm{n}}$ represents the effective nuclear charge of the core for the outer electron considered, **E** is the local electric field acting on a given ion, and **R** represents the distance from the core to any point of the wave function describing the shell of this ion. We denote the wave function for $\mathbf{E}=0$ as ψ_0, and assume that the wave function ψ of the core-shell system for $\mathbf{E}\neq 0$ may be expanded into a linear series of small perturbations in ψ_0. For this case, we introduce the variational parameter λ as

$$\psi(\lambda) = (1 + \lambda \mathbf{E} \cdot \mathbf{R})\psi_0. \tag{4}$$

By using the quantum mechanical variation method, the electronic dipole moment $\mathbf{p}_l^e$ along the l direction of the core-shell system may be expressed as[10]

$$p_l^e \cong \frac{4\langle x_3^2\rangle\langle x_l^2\rangle}{a_B}\left[1 - \frac{8\langle x_3^2\rangle^3}{a_B^2 e^2}E^2 + \frac{96\langle x_3^2\rangle^6}{a_B^4 e^4}E^4 - \frac{576\langle x_3^2\rangle^9}{a_B^6 e^6}E^6\right]E_l. \tag{5}$$

The (k,l) element of the first-order electronic polarizability tensor, the (k,l,l') element of the second-order electronic polarizability tensor (called also first-order electronic hyperpolarizability), and the (k,l,l',l'') element of the third-order electronic polarizability tensor (called also second-order electronic hyperpolarizability) are determined, respectively, as follows:[12]

$$\alpha_{kl} = \frac{\partial p_k}{\partial E_l}, \tag{6}$$

$$\beta_{kll'} = \frac{\partial^2 p_k}{\partial E_l \partial E_{l'}}, \tag{7}$$

$$\gamma_{kll'l''} = \frac{\partial^3 p_k}{\partial E_l \partial E_{l'} \partial E_{l''}}. \tag{8}$$

Following Eq. (5), α_{kl}, $\beta_{kll'}$, and $\gamma_{kll'l''}$ are described for any orbital r as

$$\alpha_{kl,r} = \alpha_{k,r}^*[\delta_{kl} - \theta_r^*(E^2\delta_{kl} + 2E_kE_l) + \xi_r^*(E^4\delta_{kl} + 4E^2E_kE_l) - \zeta_r^*(E^6\delta_{kl} + 6E^4E_kE_l)], \tag{9}$$

$$\begin{aligned}\beta_{kll',r} = \alpha_{k,r}^*[&-2\theta_r^*(E_{l'}\delta_{kl} + E_k\delta_{ll'} + E_l\delta_{kl'}) + 4\xi_r^*(E^2E_{l'}\delta_{kl} \\ &+ E^2E_k\delta_{ll'} + E^2E_l\delta_{kl'} + 2E_kE_lE_{l'}) \\ &- 6\zeta_r^*(E^4E_{l'}\delta_{kl} + E^4E_k\delta_{ll'} + E^4E_l\delta_{kl'} \\ &+ 4E^2E_kE_lE_{l'})],\end{aligned} \tag{10}$$

$$\begin{aligned}\gamma_{kll'l'',r} = \alpha_{k,r}^*[&-2\theta_r^*(\delta_{kl}\delta_{l'l''} + \delta_{kl'}\delta_{ll''} + \delta_{kl''}\delta_{ll'}) \\ &+ 4\xi_r^*(2E_kE_l\delta_{l'l''} + 2E_kE_{l'}\delta_{ll''} + 2E_kE_{l''}\delta_{ll'} \\ &+ 2E_lE_{l'}\delta_{kl''} + 2E_lE_{l''}\delta_{kl'} + 2E_{l'}E_{l''}\delta_{kl} \\ &+ E^2\delta_{kl}\delta_{l'l''} + E^2\delta_{kl'}\delta_{ll''} + E^2\delta_{kl''}\delta_{ll'}) \\ &- 6\zeta_r^*(4E^2E_kE_l\delta_{l'l''} + 4E^2E_kE_{l'}\delta_{ll''} + 4E^2E_kE_{l''}\delta_{ll'} \\ &+ 4E^2E_lE_{l'}\delta_{kl''} + 4E^2E_lE_{l''}\delta_{kl'} + 4E^2E_{l'}E_{l''}\delta_{kl} \\ &+ E^4\delta_{kl}\delta_{l'l''} + E^4\delta_{kl'}\delta_{ll''} + E^4\delta_{kl''}\delta_{ll'} + 8E_kE_lE_{l'}E_{l''})],\end{aligned} \tag{11}$$

where

$$\alpha_{k,r}^* = \frac{4\langle x_3^2\rangle_r\langle x_k^2\rangle_r}{a_B}, \tag{12}$$

$$\theta_r^* = \frac{8\langle x_3^2\rangle_r^3}{a_B^2 e^2}, \tag{13}$$

$$\xi_r^* = \frac{96\langle x_3^2\rangle_r^6}{a_B^4 e^4}, \tag{14}$$

$$\zeta_r^* = \frac{576\langle x_3^2\rangle_r^9}{a_B^6 e^6}. \tag{15}$$

In Eqs. (9)–(11), δ_{kl} represents the Kronecker symbol. We assume the first-, second-, and third-order electronic polarizabilities of a considered j ion to result from summing over all contributions of respective orbitals, namely,

$$\alpha_{kl}(j) = \sum_r \alpha_{kl,r}(j), \tag{16}$$

$$\beta_{kll'}(j) = \sum_r \beta_{kll',r}(j), \tag{17}$$

$$\gamma_{kll'l''}(j) = \sum_r \gamma_{kll'l'',r}(j). \tag{18}$$

Equations (16)–(18) can be rearranged into

$$\begin{aligned}\alpha_{kl}(j) = \alpha_k^*(j)\{&\delta_{kl} - \theta_k(j)[E^2(j)\delta_{kl} + 2E_k(j)E_l(j)] \\ &+ \xi_k(j)[E^4(j)\delta_{kl} + 4E^2(j)E_k(j)E_l(j)] \\ &- \zeta_k(j)[E^6(j)\delta_{kl} + 6E^4(j)E_k(j)E_l(j)]\},\end{aligned} \tag{19}$$

$$\begin{aligned}\beta_{kll'}(j) = \alpha_k^*(j)\{&-2\theta_k(j)[E_{l'}(j)\delta_{kl} + E_k(j)\delta_{ll'} \\ &+ E_l(j)\delta_{kl'}] + 4\xi_k(j)[E^2(j)E_{l'}(j)\delta_{kl} \\ &+ E^2(j)E_k(j)\delta_{ll'} + E^2(j)E_l(j)\delta_{kl'} \\ &+ 2E_k(j)E_l(j)E_{l'}(j)] - 6\zeta_k(j)[E^4(j)E_{l'}(j)\delta_{kl} \\ &+ E^4(j)E_k(j)\delta_{ll'} + E^4(j)E_l(j)\delta_{kl'} \\ &+ 4E^2(j)E_k(j)E_l(j)E_{l'}(j)]\},\end{aligned} \tag{20}$$

$$\begin{aligned}\gamma_{kll'l''}(j) = \alpha_k^*(j)\{&-2\theta_k(j)[\delta_{kl}\delta_{l'l''} + \delta_{kl'}\delta_{ll''} + \delta_{kl''}\delta_{ll'}] \\ &+ 4\xi_k(j)[2E_k(j)E_l(j)\delta_{l'l''} + 2E_k(j)E_{l'}(j)\delta_{ll''} \\ &+ 2E_k(j)E_{l''}(j)\delta_{ll'} + 2E_l(j)E_{l'}(j)\delta_{kl''} \\ &+ 2E_l(j)E_{l''}(j)\delta_{kl'} + 2E_{l'}(j)E_{l''}(j)\delta_{kl} + E^2(j)\delta_{kl}\delta_{l'l''} \\ &+ E^2(j)\delta_{kl'}\delta_{ll''} + E^2(j)\delta_{kl''}\delta_{ll'}] - 6\zeta_k(j) \\ &\times[4E^2(j)E_k(j)E_l(j)\delta_{l'l''} + 4E^2(j)E_k(j)E_{l'}(j)\delta_{ll''} \\ &+ 4E^2(j)E_k(j)E_{l''}(j)\delta_{ll'} + 4E^2(j)E_l(j)E_{l'}(j)\delta_{kl''} \\ &+ 4E^2(j)E_l(j)E_{l''}(j)\delta_{kl'} + 4E^2(j)E_{l'}(j)E_{l''}(j)\delta_{kl} \\ &+ E^4(j)\delta_{kl}\delta_{l'l''} + E^4(j)\delta_{kl'}\delta_{ll''} + E^4(j)\delta_{kl''}\delta_{ll'} \\ &+ 8E_k(j)E_l(j)E_{l'}(j)E_{l''}(j)]\},\end{aligned} \tag{21}$$

where

$$\alpha_k^*(j) = \sum \alpha_{k,r}^*(j), \tag{22}$$

$$\theta_k(j) = \frac{\Sigma_r \alpha^*_{k,r}(j)\theta^*_r(j)}{\Sigma_r \alpha^*_{k,r}(j)}, \tag{23}$$

$$\xi_k(j) = \frac{\Sigma_r \alpha^*_{k,r}(j)\xi^*_r(j)}{\Sigma_r \alpha^*_{k,r}(j)}, \tag{24}$$

$$\zeta_k(j) = \frac{\Sigma_r \alpha^*_{k,r}(j)\zeta^*_r(j)}{\Sigma_r \alpha^*_{k,r}(j)}. \tag{25}$$

For the calculation of the first-, second-, and third-order electronic polarizabilities of the Ba^{2+}, Ti^{4+}, and O^{2-} ions, we used the Slater-type orbitals (see Ref. 7 for more details):

$$\psi_{nlm} = \mathcal{R}_{nl}(R)Y_{lm}(\Theta,\Phi) \tag{26}$$

where n, l, and m represent the principal, azimuthal, and magnetic quantum numbers, R, Θ, and Φ are the spherical coordinates, and $\mathcal{R}_{nl}(R)$ and $Y_{lm}(\Theta,\Phi)$ represent the radial part of the wave function and the spherical harmonics, respectively.

In order to compute the coefficients $\theta_k(j)$, $\xi_k(j)$, and $\zeta_k(j)$ of a given j ion, we introduced an anisotropic effective nuclear charge of the core seen by the outer electronic layer for every ion. We then fit its components in such a way that the calculated values of the free electronic polarizabilities $\alpha^*_1(j)$, $\alpha^*_2(j)$, and $\alpha^*_3(j)$ coincide with the measured value of the free electronic polarizability $\alpha^{\exp}(j)$ of the same ion. The free electronic polarizabilities are calculated for $\mathbf{E}=0$. The effective nuclear charges of the other layers are determined by the Slater rules.[13] These fitted values have been reported in earlier work,[7] while the values of the measured $\alpha^{\exp}(j)$ and the calculated $\theta_k(j)$, $\xi_k(j)$, and $\zeta_k(j)$ are reported in Table I.

Note, that compared to former work we expand the polarizabilities here up to the third order for the reason of respecting the nonlinearities at the $BaTiO_3$ surface.

Finally, the elements of the first-, second-, and third-order electronic polarizability tensors of the j ion, which will be used in the next section, are deduced from Table I and the following three relations:

$$\begin{aligned}\alpha_{kl}(j) = \alpha^{\exp}(j)\{&\delta_{kl} - \theta_k(j)[E^2(j)\delta_{kl} + 2E_k(j)E_l(j)] \\ &+ \xi_k(j)[E^4(j)\delta_{kl} + 4E^2(j)E_k(j)E_l(j)] \\ &- \zeta_k(j)[E^6(j)\delta_{kl} + 6E^4(j)E_k(j)E_l(j)]\},\end{aligned} \tag{27}$$

$$\begin{aligned}\beta_{kll'}(j) = \alpha^{\exp}(j)\{&-2\theta_k(j)[E_{l'}(j)\delta_{kl} + E_k(j)\delta_{ll'} + E_l(j)\delta_{kl'}] \\ &+ 4\xi_k(j)[E^2(j)E_{l'}(j)\delta_{kl} + E^2(j)E_k(j)\delta_{ll'} \\ &+ E^2(j)E_l(j)\delta_{kl'} + 2E_k(j)E_l(j)E_{l'}(j)] \\ &- 6\zeta_k(j)[E^4(j)E_{l'}(j)\delta_{kl} \\ &+ E^4(j)E_k(j)\delta_{ll'} + E^4(j)E_l(j)\delta_{kl'} \\ &+ 4E^2(j)E_k(j)E_l(j)E_{l'}(j)]\},\end{aligned} \tag{28}$$

$$\begin{aligned}\gamma_{kll'l''}(j) = \alpha^{\exp}(j)\{&-2\theta_k(j)[\delta_{kl}\delta_{l'l''} + \delta_{kl'}\delta_{ll''} + \delta_{kl''}\delta_{ll'}] + 4\xi_k(j) \\ &\times[2E_k(j)E_l(j)\delta_{l'l''} + 2E_k(j)E_{l'}(j)\delta_{ll''} \\ &+ 2E_k(j)E_{l''}(j)\delta_{ll'} + 2E_l(j)E_{l'}(j)\delta_{kl''} \\ &+ 2E_l(j)E_{l''}(j)\delta_{kl'} + 2E_{l'}(j)E_{l''}(j)\delta_{kl} + E^2(j)\delta_{kl}\delta_{l'l''} \\ &+ E^2(j)\delta_{kl'}\delta_{ll''} + E^2(j)\delta_{kl''}\delta_{ll'}] - 6\zeta_k(j) \\ &\times[4E^2(j)E_k(j)E_l(j)\delta_{l'l''} + 4E^2(j)E_k(j)E_{l'}(j)\delta_{ll''} \\ &+ 4E^2(j)E_k(j)E_{l''}(j)\delta_{ll'} + 4E^2(j)E_l(j)E_{l'}(j)\delta_{kl''} \\ &+ 4E^2(j)E_l(j)E_{l''}(j)\delta_{kl'} + 4E^2(j)E_{l'}(j)E_{l''}(j)\delta_{kl} \\ &+ E^4(j)\delta_{kl}\delta_{l'l''} + E^4(j)\delta_{kl'}\delta_{ll''} + E^4(j)\delta_{kl''}\delta_{ll'} \\ &+ 8E_k(j)E_l(j)E_{l'}(j)E_{l''}(j)]\}.\end{aligned} \tag{29}$$

By analyzing the results in Table I it appears that the oxygen ion which has the highest value of the free electronic polarizability $\alpha^{\exp}$ also shows the highest values for the coefficients θ_k, ξ_k, and ζ_k, particularly those in the 3 direction which are almost doubled compared to those obtained along the 1 and 2 direction. This means that, compared to all other ions, the first-, second-, and third-order electronic polarizabilities of the oxygen ions are affected much more, particularly in the 3 direction. Note that in the following section, the local electric field $\mathbf{E}$ will be rewritten as $\mathbf{E}^{\text{loc}}$.

B. Dipole–dipole interaction

As mentioned above our model is based on the dipole–dipole interaction in correlation with the quantum mechanical orbital approximation. The model therefore accounts for the possible anisotropy in the first-, second-, and third- order electronic polarizabilities, the crystalline deformations, as well as the ionic shifts both within the bulk and near the surface. The latter are of uttermost importance when modeling the surface properties of a ferroelectric system specifically for thin ferroelectric films.

The local field acting on a given site i is given by the Lorentz relation:[14]

$$\mathbf{E}^{\text{loc}}(i) = \mathbf{E}^{\text{ext}} + \sum_j \frac{3(\mathbf{P}_j\cdot\mathbf{r}_j)\mathbf{r}_j - \mathbf{r}_j^2\mathbf{P}_j}{\mathbf{r}_j^5} + \mathbf{E}^{\text{cav}}(i). \tag{30}$$

In the last equation, $\mathbf{E}^{\text{ext}}$ represents an external electric field that generally holds as $\mathbf{E}^{\text{ext}}=\mathbf{E}^{\text{bias}}+\mathbf{E}^{\text{opt}}$, with $\mathbf{E}^{\text{bias}}$ the electric bias field, and $\mathbf{E}^{\text{opt}}$ the optical field acting on the system. The second term on the right-hand side of Eq. (30) represents the contribution to the local electric field at the considered site i by the dipole moments of all other ions j existing inside the fictitious spherical cavity of radius R^{cav} centred in i. $\mathbf{E}^{\text{cav}}$ in Eq. (30) denotes the Lorentz cavity field which is the electric field stemming from polarization charges inside the spherical cavity (as a mathematical fiction) cut out from the specimen with the reference ion as the center, as shown in Fig. 1. The cavity has radius R^{cav} and may be truncated for ions situated closer than R^{cav} to the sample surface. Usually the Lorentz cavity field, $\mathbf{E}^{\text{cav}}$, is taken to be $4\pi/3\mathbf{P}$ for an infinite medium with uniform polarization.

TABLE I. The measured free electronic polarizabilities α^{exp} (in Å^3) and the calculated values of the coefficients θ_k,ξ_k, and ζ_k (in esu CGS units) of the constituent ions of $BaTiO_3$.

j-ion	Ba^{2+}	Ti^{4+}	O^{2-}
$\alpha^{\text{exp}}(j)$	1.9460	0.1859	2.3940
$\theta_1(j)$	3.9296×10^{-15}	3.0859×10^{-16}	1.5286×10^{-14}
$\theta_2(j)$	3.9296×10^{-15}	3.0859×10^{-16}	1.5286×10^{-14}
$\theta_3(j)$	6.2384×10^{-15}	5.7175×10^{-16}	2.8585×10^{-14}
$\xi_1(j)$	0.6042×10^{-28}	3.3557×10^{-31}	0.8055×10^{-27}
$\xi_2(j)$	0.6042×10^{-28}	3.3557×10^{-31}	0.8055×10^{-27}
$\xi_3(j)$	1.0520×10^{-28}	6.9429×10^{-31}	1.6822×10^{-27}
$\zeta_1(j)$	0.5749×10^{-42}	2.0917×10^{-46}	2.4328×10^{-41}
$\zeta_2(j)$	0.5749×10^{-42}	2.0917×10^{-46}	2.4328×10^{-41}
$\zeta_3(j)$	1.0147×10^{-42}	4.3982×10^{-46}	5.1632×10^{-41}

This expression is not valid near the surface because of the nonuniformity of polarization [Fig. 1(1)] and/or because the incompleteness of the spherical cavity as sketched in Figs. 1(2) and 1(3). However, we can show that the k component of the Lorentz cavity field, $\mathbf{E}^{\text{cav}}$, is given by:

$$E_k^{\text{cav}}(i) = \pi \int_0^{\pi} P_k(\theta) f_k^{(\text{a/c})}(\theta) d\theta, \tag{31}$$

where P_k is the k-component of the polarization at point M [see Fig 1(4)]. The superscript (a/c) is used to indicate an a- or c-oriented ferroelectric domain surface. The function $f_k^{(\text{a/c})}(\theta)$ is given by (see Appendix A):

$$f_k^{(\text{a})}(\theta) = \begin{cases} f_1^{(\text{a})}(\theta) = 2\sin\theta\cos^2\theta \\ f_2^{(\text{a})}(\theta) = \sin^3\theta \\ f_3^{(\text{a})}(\theta) = \sin^3\theta \end{cases} \tag{32}$$

and

$$f_k^{(\text{c})}(\theta) = \begin{cases} f_1^{(\text{c})}(\theta) = \sin^3\theta \\ f_2^{(\text{c})}(\theta) = \sin^3\theta \\ f_3^{(\text{c})}(\theta) = 2\sin\theta\cos^2\theta. \end{cases} \tag{33}$$

The k component of the local electric field acting on i-ion sitting in the $\tilde{n}(n_x,n_y,n_z)$ unit cell (the indices (n_x,n_y,n_z) represent the coordinates of a unit cell in the whole lattice) is expressed as

$$E_k^{\text{loc}}\begin{pmatrix}\tilde{n}\\ i\end{pmatrix} = E_k^{\text{ext}} + E_k^{\text{cav}}\begin{pmatrix}\tilde{n}\\ i\end{pmatrix} + \sum_{j=1}^{5}\sum_{k'=1}^{3}\sum_{\tilde{m}} \frac{3r_{k'}\begin{pmatrix}\tilde{n},\tilde{m}\\ i,j\end{pmatrix} r_k\begin{pmatrix}\tilde{n},\tilde{m}\\ i,j\end{pmatrix} - \delta_{kk'} r^2\begin{pmatrix}\tilde{n},\tilde{m}\\ i,j\end{pmatrix}}{\left\| r\begin{pmatrix}\tilde{n},\tilde{m}\\ i,j\end{pmatrix}\right\|^5} \times p_{k'}\begin{pmatrix}\tilde{n},\tilde{m}\\ i,j\end{pmatrix}, \tag{34}$$

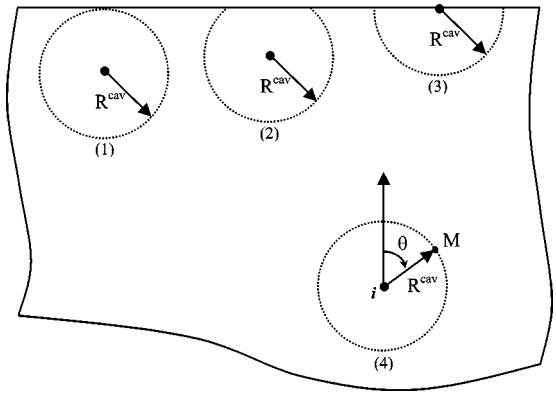

FIG. 1. Schematic of possible scenarios of the Lorentz spherical cavities located near the surface of the $BaTiO_3$ crystal.

where $\delta_{kk'}$ denotes the Kronecker symbol, and $\mathbf{r}\begin{pmatrix}\tilde{n},\tilde{m}\\ i,j\end{pmatrix}$ represents the interionic distance between the i ion in unit cell $\tilde{n}$ and the j ion in unit cell $\tilde{m}(m_x,m_y,m_z)$. The summation over j and $\tilde{m}$ covers all ions existing inside the sphere of radius R^{cav} centered in the i ion of the $\tilde{n}$ unit cell. The k component of the Lorentz cavity electric field at the i site of the $\tilde{n}$ unit cell is expressed as (see Appendix A):

for the a-surface:

$$E_k^{\text{cav}}\begin{pmatrix}\tilde{n}\\ i\end{pmatrix} = \sum_{j=1}^{5}\sum_{\tilde{m}} \frac{\pi}{v(\tilde{m})}\left[F_k^{(\text{a})}\left(\arccos\frac{r_1\begin{pmatrix}\tilde{n},\tilde{m}\\ i,1\end{pmatrix}}{R^{\text{cav}}}\right) - F_k^{(\text{a})}\left(\arccos\frac{r_1\begin{pmatrix}\tilde{n},\tilde{m}+\tilde{1}_{\text{a}}\\ i,1\end{pmatrix}}{R^{\text{cav}}}\right)\right] \times \delta_{n_y m_y}\delta_{n_z m_z} p_k\begin{pmatrix}\tilde{n},\tilde{m}\\ i,j\end{pmatrix}, \tag{35}$$

for the c-surface:

$$E_k^{\text{cav}}\begin{pmatrix}\tilde{n}\\ i\end{pmatrix} = \sum_{j=1}^{5}\sum_{\tilde{m}} \frac{\pi}{v(\tilde{m})}\left[F_k^{(\text{c})}\left(\arccos\frac{r_3\begin{pmatrix}\tilde{n},\tilde{m}\\ i,1\end{pmatrix}}{R^{\text{cav}}}\right) - F_k^{(\text{c})}\left(\arccos\frac{r_3\begin{pmatrix}\tilde{n},\tilde{m}+\tilde{1}_{\text{c}}\\ i,1\end{pmatrix}}{R^{\text{cav}}}\right)\right] \times \delta_{n_x m_x}\delta_{n_y m_y} p_k\begin{pmatrix}\tilde{n},\tilde{m}\\ i,j\end{pmatrix}. \tag{36}$$

In the last two equations, $v(\tilde{m})$ denotes the volume of the $\tilde{m}$ unit cell $[v(\tilde{m})=a^2c]$, $F_k^{(\text{a})}$ and $F_k^{(\text{c})}$ are, respectively, the primitive functions of $f_k^{(\text{a})}$ and $f_k^{(\text{c})}$, and $\tilde{m}+\tilde{1}_{\text{a}}$ and $\tilde{m}+\tilde{1}_{\text{c}}$ represent, respectively, the unit cells (m_x+1,m_y,m_z) and (m_x,m_y,m_z+1). $p_k\begin{pmatrix}\tilde{n},\tilde{m}\\ i,j\end{pmatrix}$ in Eqs. (34)–(36) is the dipole moment along the k direction which can be expressed as

$$\mathrm{P}_k\begin{pmatrix}\tilde{n},\tilde{m}\\ i,j\end{pmatrix} = \mathrm{P}_k^{e}\begin{pmatrix}\tilde{m}\\ j\end{pmatrix} + \mathrm{P}_k^{i}\begin{pmatrix}\tilde{n},\tilde{m}\\ i,j\end{pmatrix}, \tag{37}$$

with the two contributions $p_k^{\mathrm{e}}\left(\begin{smallmatrix}\tilde{m}\\ j\end{smallmatrix}\right)$ and $p_k^{\mathrm{i}}\left(\begin{smallmatrix}\tilde{n},\tilde{m}\\ i,j\end{smallmatrix}\right)$ specifying, respectively, the electronic dipole moment and the relative ionic dipole moment in the k direction of the j ion located in the $\tilde{m}$ unit cell as seen by the i ion located in the $\tilde{n}$ unit cell. These dipole moments are calculated up to a third-order development as

$$\begin{aligned} p_k^{\mathrm{e}}\begin{pmatrix}\tilde{m}\\ j\end{pmatrix} &= \sum_{l=1}^{3}\alpha_{kl}^{\mathrm{eff}}\begin{pmatrix}\tilde{m}\\ j\end{pmatrix}E_l^{\mathrm{loc}}\begin{pmatrix}\tilde{m}\\ j\end{pmatrix} \\ &+ \frac{1}{2}\sum_{l=1}^{3}\sum_{l'=1}^{3}\beta_{kll'}^{\mathrm{eff}}\begin{pmatrix}\tilde{m}\\ j\end{pmatrix}E_l^{\mathrm{loc}}\begin{pmatrix}\tilde{m}\\ j\end{pmatrix}E_{l'}^{\mathrm{loc}}\begin{pmatrix}\tilde{m}\\ j\end{pmatrix} \\ &+ \frac{1}{6}\sum_{l=1}^{3}\sum_{l'=1}^{3}\sum_{l''=1}^{3}\gamma_{kll'l''}^{\mathrm{eff}}\begin{pmatrix}\tilde{m}\\ j\end{pmatrix}E_l^{\mathrm{loc}}\begin{pmatrix}\tilde{m}\\ j\end{pmatrix}E_{l'}^{\mathrm{loc}}\begin{pmatrix}\tilde{m}\\ j\end{pmatrix}E_{l''}^{\mathrm{loc}}\begin{pmatrix}\tilde{m}\\ j\end{pmatrix} \end{aligned} \tag{38}$$

and

$$\mathrm{P}_k^{\mathrm{i}}\begin{pmatrix}\tilde{n},\tilde{m}\\ i,j\end{pmatrix} = \sum_{l=1}^{3}Z_{kl}^{*\mathrm{S}}\begin{pmatrix}\tilde{m}\\ j\end{pmatrix}e\left[\mathrm{S}_l\begin{pmatrix}\tilde{m}\\ j\end{pmatrix} - \mathrm{S}_l\begin{pmatrix}\tilde{n}\\ i\end{pmatrix}\right]. \tag{39}$$

In Eq. (38), $\alpha_{kl}^{\mathrm{eff}}\left(\begin{smallmatrix}\tilde{m}\\ j\end{smallmatrix}\right)$, $\beta_{kll'}^{\mathrm{eff}}\left(\begin{smallmatrix}\tilde{m}\\ j\end{smallmatrix}\right)$, and $\gamma_{kll'l''}^{\mathrm{eff}}\left(\begin{smallmatrix}\tilde{m}\\ j\end{smallmatrix}\right)$ represent, respectively, the (kl) element of the first-order effective electronic polarizability tensor, the (kll') element of the second-order effective electronic polarizability tensor, and the $(kll'l'')$ element of the third-order effective electronic polarizability tensor of the j ion located in the $\tilde{m}$ unit cell, given by Eqs. (B7)–(B9) in Appendix B. In Eq. (39) $Z_{kl}^{*s}\left(\begin{smallmatrix}\tilde{m}\\ j\end{smallmatrix}\right)$ denotes the (kl) component of the static effective charge tensor of the j ion located in the $\tilde{m}$ unit cell as given at the beginning of Sec. III, and $s_l(i)$ and $s_l(j)$ denote, respectively, the shifts of the i and j ions along the l direction. Thus the local field present along the k direction acting on ion i of the $\tilde{n}$ unit cell can be written as

$$\sum_{j=1}^{5}\sum_{l=1}^{3}\sum_{\tilde{m}}S_{kl}\begin{pmatrix}\tilde{n},\tilde{m}\\ i,j\end{pmatrix}E_l^{\mathrm{loc}}\begin{pmatrix}\tilde{m}\\ j\end{pmatrix} = Q_k\begin{pmatrix}\tilde{n}\\ i\end{pmatrix}, \tag{40}$$

with

$$\begin{aligned} S_{kl}\begin{pmatrix}\tilde{n},\tilde{m}\\ i,j\end{pmatrix} &= \delta_{kl}\delta_{ij}\delta_{\tilde{n}\tilde{m}} - \sum_{k'=1}^{3}T_{kk'}\begin{pmatrix}\tilde{n},\tilde{m}\\ i,j\end{pmatrix}\left[\alpha_{k'l}^{\mathrm{eff}}\begin{pmatrix}\tilde{m}\\ j\end{pmatrix} + \sigma_{k'l}^{\mathrm{eff}}\begin{pmatrix}\tilde{m}\\ j\end{pmatrix}\right. \\ &\left. + \rho_{k'l}^{\mathrm{eff}}\begin{pmatrix}\tilde{m}\\ j\end{pmatrix}\right], \end{aligned} \tag{41}$$

and

$$Q_k\begin{pmatrix}\tilde{n}\\ \tilde{i}\end{pmatrix} = E_k^{\mathrm{ext}} + \sum_{j=1}^{5}\sum_{k'=1}^{3}\sum_{\tilde{m}}T_{kk'}\begin{pmatrix}\tilde{n},\tilde{m}\\ i,j\end{pmatrix}p_{k'}^{\mathrm{i}}\begin{pmatrix}\tilde{n},\tilde{m}\\ i,j\end{pmatrix}, \tag{42}$$

where for the a-surface:

$$\begin{aligned} T_{kk'}\begin{pmatrix}\tilde{n},\tilde{m}\\ i,j\end{pmatrix} &= \frac{3r_{k'}\begin{pmatrix}\tilde{n},\tilde{m}\\ i,j\end{pmatrix}r_k\begin{pmatrix}\tilde{n},\tilde{m}\\ i,j\end{pmatrix} - \delta_{kk'}r^2\begin{pmatrix}\tilde{n},\tilde{m}\\ i,j\end{pmatrix}}{\left\|\mathbf{r}\begin{pmatrix}\tilde{n},\tilde{m}\\ i,j\end{pmatrix}\right\|^5} \\ &+ \frac{\pi}{v(\tilde{m})}\left[F_{k'}^{(\mathrm{a})}\left(\arccos\frac{r_1\begin{pmatrix}\tilde{n},\tilde{m}\\ i,j\end{pmatrix}}{R^{\mathrm{cav}}}\right)\right. \\ &\left. - F_{k'}^{(\mathrm{a})}\left(\arccos\frac{r_1\begin{pmatrix}\tilde{n},\tilde{m}+\tilde{1}_{\mathrm{a}}\\ i,j\end{pmatrix}}{R^{\mathrm{cav}}}\right)\right]\delta_{n_ym_y}\delta_{n_zm_z}\delta_{kk'}, \end{aligned} \tag{43}$$

and for the c-surface:

$$\begin{aligned} T_{kk'}\begin{pmatrix}\tilde{n},\tilde{m}\\ i,j\end{pmatrix} &= \frac{3r_{k'}\begin{pmatrix}\tilde{n},\tilde{m}\\ i,j\end{pmatrix}r_k\begin{pmatrix}\tilde{n},\tilde{m}\\ i,j\end{pmatrix} - \delta_{kk'}r^2\begin{pmatrix}\tilde{n},\tilde{m}\\ i,j\end{pmatrix}}{\left\|\mathbf{r}\begin{pmatrix}\tilde{n},\tilde{m}\\ i,j\end{pmatrix}\right\|^5} \\ &+ \frac{\pi}{v(\tilde{m})}\left[F_{k'}^{(\mathrm{c})}\left(\arccos\frac{r_3\begin{pmatrix}\tilde{n},\tilde{m}\\ i,j\end{pmatrix}}{R^{\mathrm{cav}}}\right) - F_{k'}^{(\mathrm{c})}\right. \\ &\left.\times\left(\arccos\frac{r_3\begin{pmatrix}\tilde{n},\tilde{m}+\tilde{1}_{\mathrm{a}}\\ i,j\end{pmatrix}}{R^{\mathrm{cav}}}\right)\right]\delta_{n_ym_y}\delta_{n_zm_z}\delta_{kk'}. \end{aligned} \tag{44}$$

$$\sigma_{k'l}^{\mathrm{eff}}\begin{pmatrix}\tilde{m}\\ j\end{pmatrix} = \frac{1}{2}\sum_{l'=1}^{3}\beta_{k'll'}^{\mathrm{eff}}\begin{pmatrix}\tilde{m}\\ j\end{pmatrix}E_{l'}^{\mathrm{loc}}\begin{pmatrix}\tilde{m}\\ j\end{pmatrix}, \tag{45}$$

and

$$\rho_{k'l}^{\mathrm{eff}}\begin{pmatrix}\tilde{m}\\ j\end{pmatrix} = \frac{1}{6}\sum_{l'=1}^{3}\sum_{l''=1}^{3}\gamma_{k'll'l''}^{\mathrm{eff}}\begin{pmatrix}\tilde{m}\\ j\end{pmatrix}E_{l'}^{\mathrm{loc}}\begin{pmatrix}\tilde{m}\\ j\end{pmatrix}E_{l''}^{\mathrm{loc}}\begin{pmatrix}\tilde{m}\\ j\end{pmatrix}. \tag{46}$$

The second-rank tensors $\tilde{\sigma}^{\mathrm{eff}}\left(\begin{smallmatrix}\tilde{m}\\ j\end{smallmatrix}\right)$ and $\tilde{\rho}^{\mathrm{eff}}\left(\begin{smallmatrix}\tilde{m}\\ j\end{smallmatrix}\right)$ are introduced in order to represent, respectively, the effect of the second-order effective electronic polarizability $\tilde{\beta}^{\mathrm{eff}}\left(\begin{smallmatrix}\tilde{m}\\ j\end{smallmatrix}\right)$ tensor (third-rank tensor) and the third-order effective electronic polarizability $\tilde{\gamma}^{\mathrm{eff}}\left(\begin{smallmatrix}\tilde{m}\\ j\end{smallmatrix}\right)$ tensor (fourth-rank tensor).

From Eqs. (40) and (41) it appears that the components of the local electric field depend on those of the first-, second-, and third-order effective electronic polarizabilities, while these, in turn, also depend on the electric field components through Eqs. (B7), (B8), (B9), (27), (28), and (29). This mutual dependence between the first-, second-, and third-order electronic polarizabilities (orbital approximation) on one hand, and their dependence on the electric field (dipole–dipole interaction) on the other hand, makes a self-consistent calculation necessary.

By solving Eq. (40) we obtain $E_l^{\mathrm{loc}}\binom{\tilde{m}}{j}$, the l component of the local electric field of the j ion located in the $\tilde{m}$ unit cell. The total polarization, $P_k(\tilde{m})$, of the $\tilde{m}$ unit cell is expressed as

$$P_k(\tilde{m}) = \frac{1}{v(\tilde{m})}\sum_{j=1}^{5}\left[p_k^{\mathrm{e}}\binom{\tilde{m}}{j} + \sum_{l=1}^{3} Z_{kl}^{*\mathrm{s}}\binom{\tilde{m}}{j} e\cdot s_l\binom{\tilde{m}}{j}\right]. \tag{47}$$

The connection between the optical dielectric constant $\varepsilon_{kl'}^{\mathrm{opt}}(\tilde{m})$, electronic dipole moments $p_k^{\mathrm{e}}\binom{\tilde{m}}{j}$, and the optical electric field $E_{l'}^{\mathrm{opt}}$ is expressed in the following way:

$$\varepsilon_{kl'}^{\mathrm{opt}}(\tilde{m}) = \delta_{kl'} + \frac{4\pi}{v(\tilde{m})}\sum_{j=1}^{5}\frac{\partial p_k^{\mathrm{e}}\binom{\tilde{m}}{j}}{\partial E_{l'}^{\mathrm{opt}}}. \tag{48}$$

By using Eq. (38), the term $\partial p_k^{\mathrm{e}}\binom{\tilde{m}}{j}/\partial E_{l'}^{\mathrm{opt}}$ can be written as

$$\frac{\partial p_k^{\mathrm{e}}\binom{\tilde{m}}{j}}{\partial E_{l'}^{\mathrm{opt}}} = \sum_{l=1}^{3}\left[\alpha_{kl}^{\mathrm{eff}}\binom{\tilde{m}}{j} + 2\sigma_{kl}^{\mathrm{eff}}\binom{\tilde{m}}{j} + 3\rho_{kl}^{\mathrm{eff}}\binom{\tilde{m}}{j}\right] \times \frac{\partial E_l^{\mathrm{loc}}\binom{\tilde{m}}{j}}{\partial E_{l'}^{\mathrm{opt}}}. \tag{49}$$

Note that $\partial E_l^{\mathrm{loc}}\binom{\tilde{m}}{j}/\partial E_{l'}^{\mathrm{opt}}$ which represents the local electric field induced along the l direction of the j ion located in the $\tilde{m}$ unit cell by unit of the l' component of the optical electric field, can be obtained by solving the following equation, deduced from Eq. (34):

$$\sum_{j=1}^{5}\sum_{l=1}^{3}\sum_{\tilde{m}} S_{kl}^{*}\binom{\tilde{n},\tilde{m}}{i,j}\frac{\partial E_l^{\mathrm{loc}}\binom{\tilde{m}}{j}}{\partial E_{l'}^{\mathrm{opt}}} = \delta_{kl'}, \tag{50}$$

where

$$S_{kl}^{*}\binom{\tilde{n},\tilde{m}}{i,j} = \delta_{kl}\delta_{ij}\delta_{\tilde{n}\tilde{m}} - \sum_{k'=1}^{3} T_{kk'}\binom{\tilde{n},\tilde{m}}{i,j} \times\left[\alpha_{k'l}^{\mathrm{eff}}\binom{\tilde{m}}{j} + 2\sigma_{k'l}^{\mathrm{eff}}\binom{\tilde{m}}{j} + 3\,\rho_{k'l}^{\mathrm{eff}}\binom{\tilde{m}}{j}\right]. \tag{51}$$

In electromagnetic theory[15] the index ellipsoid (also called the optical indicatrix) in a given coordinate system is written as

$$\sum_{k=1}^{3}\sum_{l=1}^{3}\eta_{kl}^{\mathrm{opt}}x_k x_l = 1, \tag{52}$$

where $\tilde{\eta}^{\mathrm{opt}}$ represents the optical dielectric impermeability tensor of the medium $\tilde{\eta}^{\mathrm{opt}} = (\tilde{\varepsilon}^{\mathrm{opt}})^{-1}$, and x_1, x_2, and x_3 are the coordinates of an arbitrary point N on the periphery of the ellipsoid in the coordinate system. In this case the refractive index of the light polarized along the *ON* direction (O is the center of the ellipsoid) is $n = \sqrt{(x_1^2 + x_2^2 + x_3^2)}$.

In the special case of light being polarized along the k direction, the refractive index thus becomes:

$$n_k = \frac{1}{\sqrt{\eta_{kk}^{\mathrm{opt}}}}. \tag{53}$$

III. RESULTS AND DISCUSSION

The calculation of the spontaneous polarization and refractive indices is carried out for both *a*- and *c*-domain areas in tetragonal $BaTiO_3$ at room temperature by using the lattice parameters and spontaneous ionic shifts given in Ref. 11. As static effective charges, we use the data published in a recent theoretical work devoted to the quantitative study of successive phase transitions in $BaTiO_3$:[16–18] $Z_{33}^{*\mathrm{s}}(Ba^{2+}) = 1.437$, $Z_{33}^{*\mathrm{s}}(Ti^{4+}) = 2.063$, $Z_{33}^{*\mathrm{s}}(O_{x,y}^{2-}) = -1.200$, and $Z_{33}^{*\mathrm{s}}(O_z^{2-}) = -1.100$. It is noteworthy that, for symmetry reasons, the static effective charge tensors of the constituent ions of tetragonal $BaTiO_3$ have to be diagonal, and consequently the nondiagonal elements $Z_{kl}^{*\mathrm{s}}$ are zero. Moreover, the components $Z_{11}^{*\mathrm{s}}$ and $Z_{22}^{*\mathrm{s}}$ of the static effective charge tensors have no effect in the calculation because the static effective charges are coupled with the ionic shifts which are parallel to the three-direction. It is assumed that these magnitudes (lattice parameters, static effective charges and ionic shifts) are valid both near the surface and in the bulk. In this computation we have to solve Eqs. (40) and (50), which are in fact two sets of equations. By considering only the 86 unit cell monolayers nearest to the surface and taking into account that all unit cells in the same monolayer have the same properties, the number of equations in each set can be reduced to $3\times5\times86 = 1290$ equations.

Now we present and discuss the results obtained for the spontaneous polarization in the $\tilde{n}$ unit cell, $P^{\mathrm{spn}}(\tilde{n})$. $P^{\mathrm{spn}}(\tilde{n})$ is ascribed to the unit cell (and not to individual ions) and is defined as the total dipole moment (in the unit cell) per volume. The components $P_k(\tilde{n})$ are deduced from Eq. (47) in the absence of any external field. The calculation shows that the values of the spontaneous polarization near the *a*- and *c*-surface of tetragonal $BaTiO_3$ at room temperature along the 1 and 2 direction are exactly zero. On the other hand, the 3 component of the spontaneous polarization $P_3^{\mathrm{spn}}(\tilde{n})$ is nonzero and is reported in Fig. 2 for the *a*-surface (both BaO- and TiO_2-terminated), and in Fig. 3 for the *c*-surface (both BaO- and TiO_2-terminated). We see that the spontaneous polarization for the BaO- terminated *a*-surface does not show any remarkable changes near the surface except the small decrease presented by the last unit cell closest to the surface (see Fig. 2). The behavior is completely different for a TiO_2-terminated *a*-surface for which the spontaneous polarization shows a small decrease when approaching the surface for $R^{\mathrm{cav}} = 40$ Å and $R^{\mathrm{cav}} = 80$ Å. In both cases the decrease of P^{spn} near the surface measures less than 10%. This decrease is far smaller than that presented near *c*-surfaces, which reaches 57% (see Fig. 3). As shown in Fig. 3, the behavior of the spontaneous polarization near the *c*-surface is the same

for the four distinguished cases. The only difference manifests in the effective value of the spontaneous polarization of the unit cell monolayer closest to the surface, which is smaller for BaO-terminated (both c^- and c^+)-surfaces than for TiO_2-terminated (both c^- and c^+)-surfaces. However, in all cases the values of the spontaneous polarization near and far away from the *c*-surface (inside the bulk) do not change when varying R^{cav}; only in between the bulk and the surface are changes observed. In fact the larger R^{cav}, the more accurate is the calculation since more interacting unit cells are considered. However, increasing R^{cav} further in our calculation is currently impossible due to extremly long computation time.

Figures 4 and 5 report the calculated values for the refractive indices ascribed to each unit cell near the *a*-surface (both BaO- and TiO_2-terminated) and $c^{\pm}$-surfaces (both BaO- and TiO_2-terminated) of tetragonal $BaTiO_3$ at room temperature, respectively. Note that the calculated results are displayed as the discrete values for the refractive indices making sense on the unit cell bases only (and not on the ionic scale). For *a*-surfaces (either BaO- or TiO_2-terminated), the n_1 refractive index, which corresponds to light polarized perpendicular to the surface, undergoes a very stong decrease when approching the surface (Fig. 4). Values range from 2.38 inside the bulk (far away from the surface) to ~1.75 close to the surface. However, the change undergone by the refractive indices n_2 and n_3, corresponding to light polarized in the plane parallel to the *a*-surface, is very small. This change manifests in a decrease in both refractive indices when approaching the surface, and it is more pronounced for TiO_2-terminated than for BaO- terminated surfaces. When approching the *c*-surface (either c^+ or c^- and either BaO- or TiO_2-terminated), the refractive index n_3, corresponding to light polarized perpendicular to the sample surface, undergoes a decrease similar to that undergone by n_1 near the *a*-surface. It decreases from 2.32 inside the bulk (far away from the surface) to ~1.73 close to the surface (Fig. 5). Note that near the *c*-surface the refractive indices n_1 and n_2 coincide with each other (i.e., $n_1=n_2$). These two refractive indices remain almost constant when approaching the BaO-terminated $c^{\pm}$-surface. However, their change near the TiO_2-terminated $c^{\pm}$-surface is apparent and is more pronounced for $R^{cav}=40$ Å than for $R^{cav}=80$ Å.

The unit cell monolayer closest to the surface for all studied *a*-and *c*-surfaces presents an exception with respect to the other unit cell monolayers for the refractive indices corresponding to light being polarized parallel to the surface (i.e., n_2 and n_3 for *a*-surface, and n_1 and n_2 for *c*-surface). This exception manifests in the discontinuous decrease of the concerned refractive indices of the unit cell monolayer closest to the sample surface.

Far away from the surface and for whatever the value chosen for R^{cav}, the crystal possesses only two refractive indices, the ordinary refractive index n_o (which coincides with $n_1=n_2$), and the extraordinary refractive index n_e (which is n_3). The calculated values of these indices are $n_o=2.385$ and $n_e=2.315$, respectively, which are in good agreement with experimental data ($n_o=2.398$ and $n_e=2.312$) given by Johnston and Weingart[20] for single-domain tetragonal $BaTiO_3$ at room temperature. Nevertheless, the material behaves near the surface either like a uniaxial negative material with high optical birefringence, $\delta n \sim 0.55$ (for a *c*-surface) or like a biaxial material having three different refractive indices (near an *a*-surface).

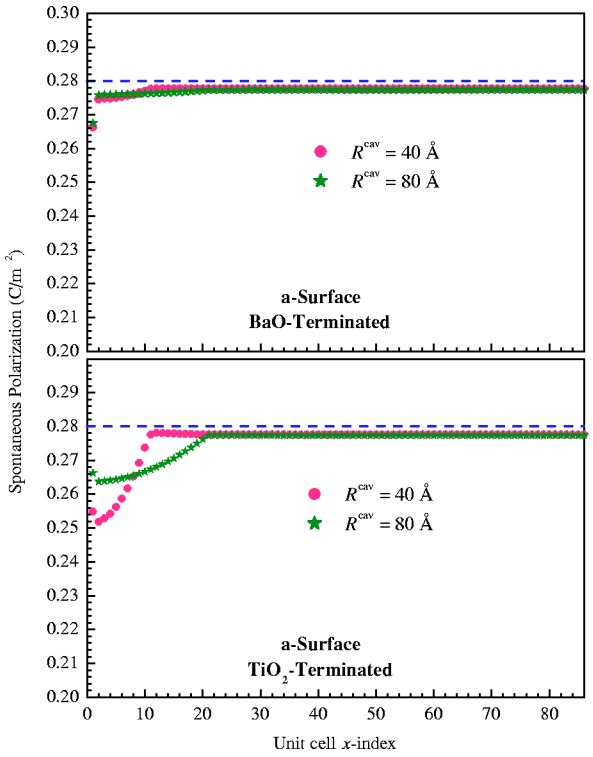

FIG. 2. (Color online) Variation of the spontaneous polarization near the *a*-surface (both BaO- and TiO_2 -terminated) of tetragonal $BaTiO_3$. Results are computed at room temperature with $R^{cav}=40$ Å and $R^{cav}=80$ Å. The dashed line represents the single crystal measured spontaneous polarization according to Cudney (Ref. 19).

As mentioned before, it is not possible to perform the present study of the surface effect on the electrical and optical properties of tetragonal $BaTiO_3$ for values of R^{cav} larger than 80 Å due to the extremely long computation time. However, computation was done for some other values of R^{cav} (20, 40, 60, 70, and 80 Å) in the case of BaO-terminated c^--surface in order to figure out the convergence tendency of both the spontaneous polarization and refractive indices with R^{cav}. These results are reported in Fig. 6, and show that both the spontaneous polarization and refractives indices, which keep their behavior near the surface unchangeable with R^{cav}, have a tendency to convergence when increasing R^{cav} because the curves approach each others for high values of R^{cav}. These theoretical calculations show that the behavior of the spontaneous polarization or the refractive indices is almost the same, whatever the value of the spherical cavity radius R^{cav}. The spontaneous polarization is always parallel to the *c*-axis and its value decreases strongly near the *c*-surface. On the other hand, the refractive index corresponding to light polarized perpendicular to the sample surface undergoes an important change near the surface.

In the next part, which is restricted to tetragonal $BaTiO_3$ single crystals, we present and discuss the dependence of the electrical and optical properties on some microscopic mag-

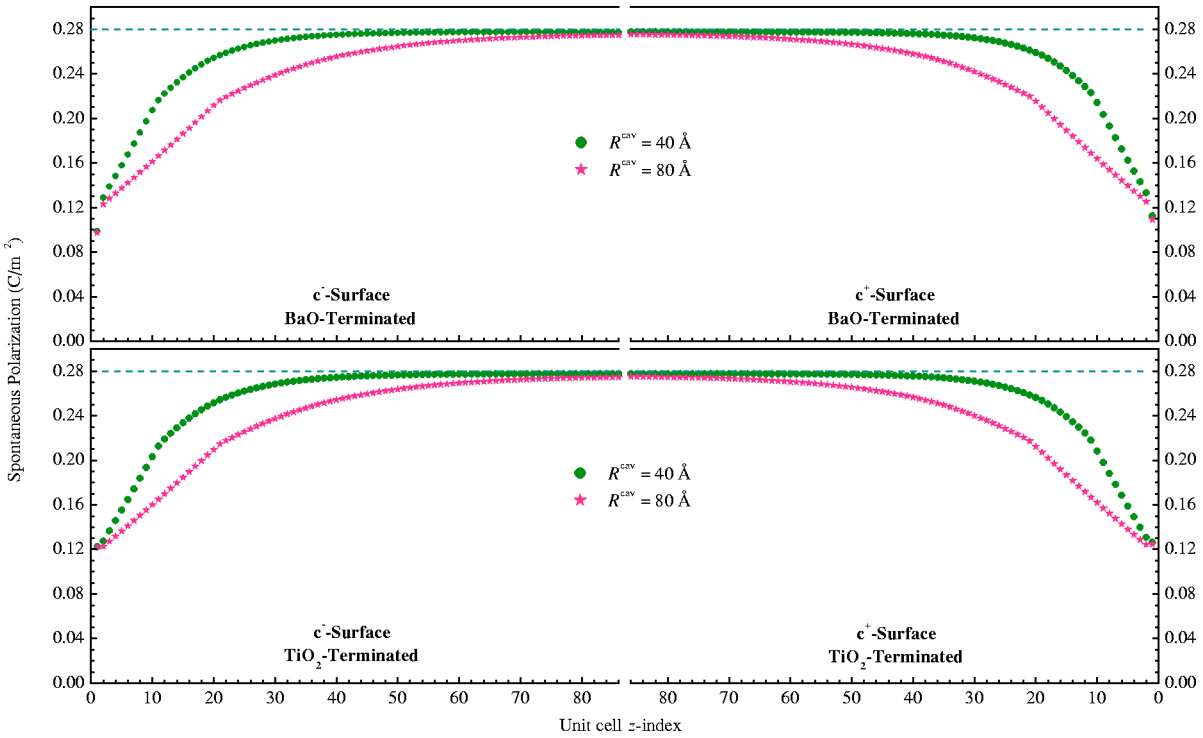

FIG. 3. (Color online) Variation of the spontaneous polarization near the c^+-and c^--surfaces (both BaO- and TiO_2-terminated) of tetragonal $BaTiO_3$. Results are computed at room temperature with $R^{cav}=40$ Å and $R^{cav}=80$ Å. The dashed line represents the single crystal measured spontaneous polarization according to Cudney (Ref. 19).

nitudes used in this model like the order of the electronic polarizability taken into account in the calculation, and also the static effective charges of the constituent ions. In the above reported calculations, we took into account the effects of both the first-, second-, and third-order electronic polarizabilities. In order to study the contribution of each of these three electronic polarizabilities, we report in Table II the calculated values of the spontaneous polarization, refractive indices, and optical birefringence of $BaTiO_3$ single crystals at room temperature for different orders of expansion of the electronic polarizabilities. From these results, it appears that the main contributor to the optical properties is the first-order electronic polarizability. For the spontaneous polarization, in which the ionic polarization contributes by 28.94%, the first-, second-, and third-order electronic polarizabilities contribute by 62.58, 10.25, and -1.77%, respectively. The fact that the contribution of the third-order electronic polarizability to the spontaneous polarization is lower than 2% (in absolute numbers) means that the expansion of the electronic polarizabilities up the third order is enough for obtaining accurate results for both electrical and optical properties.

Among the microscopic magnitudes upon which the electrical and optical properties strongly depend are the static effective charges of the constituent ions. Table III reports some sets of the static effective charges that are found in literature, and the corresponding calculated values of the spontaneous polarization, refractive indices, and optical birefringence of tetragonal $BaTiO_3$ single crystals at room temperature. We see that the values of all computed magnitudes undergo important changes when changing the values of static effective charges. Make sure not to confuse the *static* effective charges used in our calculations with the *dynamic* effective charges (called also the *Born* effective charges or *transverse* effective charges) used usually for lattice dynamics calculations.[25–29] While the components of the static effective charge tensors (Z^{*s}_{kl}) of the constituent ions are con-

TABLE II. The spontaneous polarization (in C/m^2), refractive indices, and optical birefringence of $BaTiO_3$ single crystals at room temperature calculated as function of the orders of the electronic polarizabilities.

Electronic polarizabilities	P^{spn}	n_o	n_e	δn
No polarizability[a]	0.0802[b]	1[c]	1[c]	0
first-order[d]	0.2536	2.3854	2.3153	−0.0702
first- and second-order[e]	0.2820	2.3846	2.3140	−0.0706
first- to third-order[f]	0.2771	2.3848	2.3150	−0.0698

[a]Here, all orders of the electronic polarizabilitiy are ignored and then the ions are considered as rigid (nonpolarizable).
[b]This value represents the ionic contribution to the spontaneous polarization.
[c]The refractive index of the nonpolarizable medium coincides with that of the vacuum.
[d]In this case only the first-order electronic polarizability ($\tilde{\alpha}$) is considered. The terms with ξ and ζ in the expression of $\alpha_{kl}(j)$ [Eq. (27)] are omitted.
[e]In this case both the first- ($\tilde{\alpha}$) and second-order ($\tilde{\beta}$) electronic polarizabilities are considered. The terms with ζ in the expression of $\alpha_{kl}(j)$ [Eq. (27)] and $\beta_{kll'}(j)$ [Eq. (28)] are omitted.
[f]In this case all three orders of the electronic polarizabilities ($\tilde{\alpha}$, $\tilde{\beta}$, and $\tilde{\gamma}$) are considered.

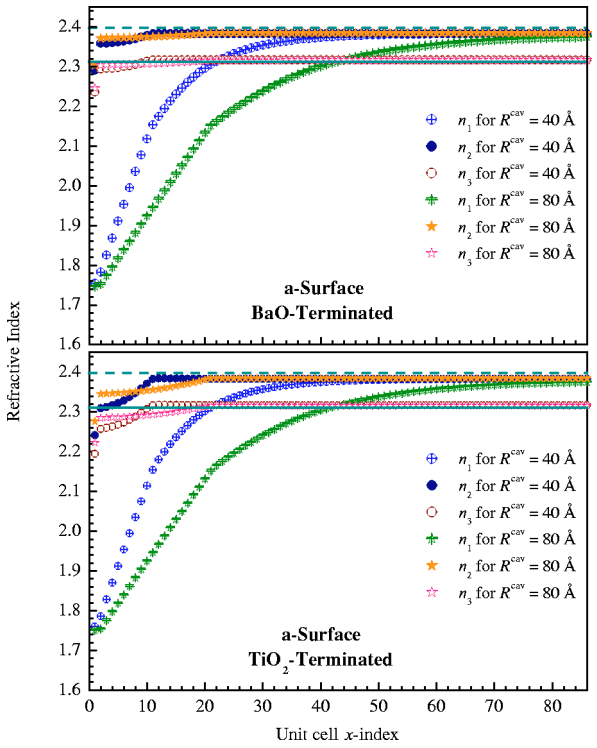

FIG. 4. (Color online) Variation of the refractive indices near the *a*-surface (both BaO- and TiO_2-terminated) of tetragonal $BaTiO_3$. Results are computed at room temperature with $R^{cav}=40$ Å and $R^{cav}=80$ Å. The dashed and solid lines represent measured single crystal values of the ordinary and extraordinary refractive indices according to Johnston and Weingart (Ref. 20).

nected to the polarization of the crystal through Eq. (47), the components of their dynamic effective charge tensors (Z^{*d}_{kl}) are connected, in turn, to the polarization through the following equation:[29]

$$Z^{*d}_{kl}\left(\begin{matrix}\dot{m}\\ j\end{matrix}\right)=\frac{v(\tilde{m})}{e}\cdot\frac{\partial P_k(\tilde{m})}{\partial s_l\left(\begin{matrix}\tilde{m}\\ j\end{matrix}\right)}. \tag{54}$$

However, the elements of the dynamic effective charge tensor of a given ion are linked to the elements of the static effective charges tensors of the other ions in the same unit cell by the following equation:

$$Z^{*d}_{kl}\left(\begin{matrix}\tilde{m}\\ j\end{matrix}\right)=Z^{*s}_{kl}\left(\begin{matrix}\tilde{m}\\ j\end{matrix}\right)+\frac{1}{e}\sum_{j'=1}^{5}\frac{\partial p^{e}_{k}\left(\begin{matrix}\tilde{m}\\ j'\end{matrix}\right)}{\partial s_l\left(\begin{matrix}\tilde{m}\\ j\end{matrix}\right)}. \tag{55}$$

The right-hand side of the last equation has the same sign as the static effective charge Z^{*s}_{kl} of the *j* ion, because a positive shift of a positively charged ion induces an increase of both the ionic and electronic dipole moments while a positive shift of a negatively charged ion induces a decrease of both the ionic and electronic dipole moments. This is why the elements of the dynamic effective charge tensor of a given ion are larger than the corresponding ones of its static effective charge tensor.[28,30–32]

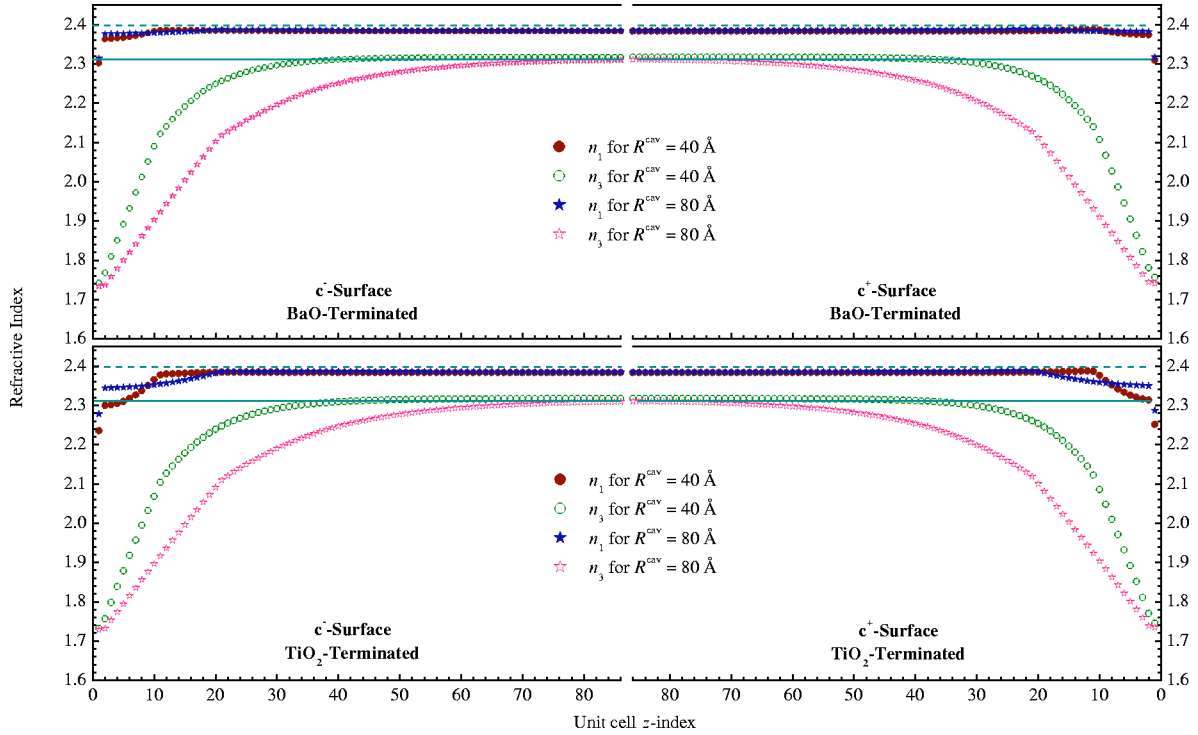

FIG. 5. (Color online) Variation of the refractive indices near the c^+- and c^--surfaces (both BaO- and TiO_2-terminated) of tetragonal $BaTiO_3$. Results are computed at room temperature with $R^{cav}=40$ Å and $R^{cav}=80$ Å. The dashed and solid lines represent the single crystal measured values, respectively, of the ordinary and extraordinary refractive indices according to Johnston and Weingart (Ref. 20).

IV. CONCLUSIONS

By using a microscopic model taking into account a quantum method based upon the orbital approximation and the dipole–dipole interaction due to the local electric field acting on the constituent ions, we calculated the electric and optical properties near the surface of tetragonal $BaTiO_3$ at room temperature. The study concerns all types of surfaces either being *a* or $c^{\pm}$-surfaces (both BaO and TiO_2 terminated). The calculations show that the spontaneous polarization and refractive indices have the same behavior when changing the spherical cavity radius R^{cav}. However, the spontaneous polarization decreases near the $c^{\pm}$-surfaces and behaves quite similar to recent theoretical work based on Landau[33,34] and Landau–Ginzburg–Devonshire thermodynamic theory,[35] and also to shell model calculations for ultrathin films.[36] Our model also allows us to compute the spontaneous polarization near the *a*-surfaces, which holds almost constant even very close the surface. Furthermore, the $BaTiO_3$ behaves like a biaxial crystal resulting in dramatic changes of the refractive index n_1 near the *a*-surfaces and behaving like a uniaxial crystal resulting in dramatic changes of the refractive index n_3 near the $c^{\pm}$-surfaces. Therefore, the surface effect has a tendency to reduce the refractive indices. This effect might be the main origin of the reduction of refractive indices of $BaTiO_3$ films observed in recent experimental work.[37,38] The surface is expected to have more important influence on the reduction of both spontaneous polarization and refractive indices in thin films where the effect of two surfaces has to be considered.

ACKNOWLEDGMENTS

Financial support of this work by the "Deutsche Forschungsgemeinschaft" under Grant Nos. EN 434/7, EN 434/2, EN 434/13–1, GR 1288/7–1, and EN 434/15–1 is gratefully acknowledged.

APPENDIX A: LORENTZ CAVITY FIELD EXPRESSION

The expression of the local electric field created by the spherical Lorentz cavity will be demonstrated in this appendix for the *c*-surface. The one corresponding to the *a*-surface can be evaluated correspondingly. However, near the *c*-surface, the polarization **P** on the Lorentz cavity surface is not uniform and depends on *z* (or θ by using the spherical coordinates). The element of electric field created in the center *i* (see Fig. 7) by the charges located in the area element $d\mathbf{S}$ with

$$d\mathbf{S} = (R^{cav})^2 \sin\theta\, d\theta\, d\varphi \cdot \mathbf{n} \tag{A1}$$

is denoted as

$$\delta\mathbf{E}^{cav} = (\mathbf{P}\cdot\mathbf{n}) \cdot \sin\theta\, d\theta\, d\varphi \cdot \mathbf{n}. \tag{A2}$$

n is the unit vector normal to the surface and the product $\mathbf{P}\cdot\mathbf{n}$ represents the charge density in the area element $d\mathbf{S}$.

By taking into account that the polarization depends only on θ, the components of $\delta\mathbf{E}^{cav}$ can be expressed as

$$\begin{cases} \delta E_1^{cav} = \pi P_1(\theta)\sin^3\theta\, d\theta \\ \delta E_2^{cav} = \pi P_2(\theta)\sin^3\theta\, d\theta \\ \delta E_3^{cav} = 2\pi P_3(\theta)\sin\theta\cos^2\theta\, d\theta. \end{cases} \tag{A3}$$

Thus,

TABLE III. The spontaneous polarization (in C/m^2), refractive indices, and optical birefringence of $BaTiO_3$ single crystals at room temperature calculated by using some sets of static effective charges found in litirature. Measured values are also reported for comparison.

The set of static effective charges[a]				The corresponding calculated magnitudes			
Reference	Ba^{2+}	Ti^{4+}	$O^{2-}_{x,y,z}$	P^{spn}	n_o	n_e	δn
Freire[b]	1.582	2.678	−1.420	0.3504	2.3784	2.2742	−0.1042
Gervais[c]	1.480	2.720	−1.400	0.3522	2.3780	2.2713	−0.1067
Pinto[d]	1.730	2.450	−1.360	0.3277	2.3809	2.2895	−0.0914
Kuroiwa[e]	1.900	1.900	−1.1/−1.6[f]	0.2842	2.3854	2.3198	−0.0656
Toumanari[g]	1.437	2.063	−1.2/−1.1[h]	0.2771	2.3848	2.3150	−0.0698
Measured				0.2800[i]	2.3980[j]	2.3120[j]	−0.0860[j]

[a]As mentioned at the beginning of this section, only the third component (Z^{*s}_{33}) of the static effective charge tensor contributes in the calculation because the static effective charges are coupled with the ionic shifts which are parallel to the three-direction in the tetragonal $BaTiO_3$.
[b]Reference 21.
[c]Reference 22.
[d]Reference 23. This set of static effective charges does not respect the rule of neutrality [$\Sigma_{j=1}^{5} Z^{*s}(j)=0$].
[e]Reference 24. In this set of static effective charges $Z^{*s}(Ba^{2+})$ has the same value as $Z^{*s}(Ti^{4+})$ which is far expected being seen that $Z(Ba^{2+})=2$ and $Z(Ti^{4+})=4$, where $Z(j)$ is the nominal charge of the *j* ion.
[f]−1.1 is the static effective charge of $O^{2-}_{x,y}$ and −1.6 is that of O^{2-}_{z}.
[g]This set of static effective charges is the same used for the study of $BaTiO_3$ surfaces in this work.
[h]−1.2 is the static effective charge of $O^{2-}_{x,y}$ and −1.1 is that of O^{2-}_{z}.
[i]Reference 19.
[j]Reference 20.

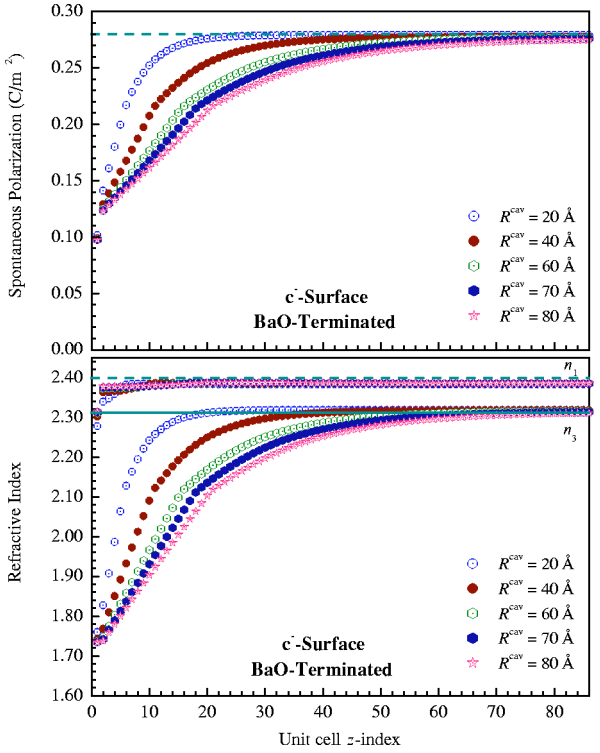

FIG. 6. (Color online) Variation of the spontaneous polarization (top curve) and refractive indices (bottom curve) near the BaO-terminated c^--surface of tetragonal $BaTiO_3$. Results are computed at room temperature for 5 values of R^{cav}: 20, 40, 60, 70, and 80 Å. The dashed line in the top curve represents the single crystal measured spontaneous polarization according to Cudney[19] and the dashed and solid lines in the bottom curve represent the single crystal measured values, respectively, of the ordinary and extraordinary refractive indices according to Johnston and Weingart.[20]

$$E_k^{cav} = \pi \int_0^{\pi} P_k(\theta) f_k^{(c)}(\theta) d\theta, \tag{A4}$$

with

$$f_k^{(c)}(\theta) = \begin{cases} f_1^{(c)}(\theta) = \sin^3\theta \\ f_2^{(c)}(\theta) = \sin^3\theta \\ f_3^{(c)}(\theta) = 2\sin\theta\cos^2\theta. \end{cases} \tag{A5}$$

Now, let us assume that the polarization **P** is constant over each unit cell monolayer, **P** is constant between $r_3\left(\begin{smallmatrix}\tilde{n},\tilde{m}\\ i,1\end{smallmatrix}\right)$ and $r_3\left(\begin{smallmatrix}\tilde{n},\tilde{m}+\tilde{1}_c\\ i,1\end{smallmatrix}\right)$ (see Fig. 7). Therefore, the k component of the Lorentz cavity electric field of the i ion in the $\tilde{n}$ unit cell can be computed as

$$E_k^{cav}\begin{pmatrix}\tilde{n}\\ i\end{pmatrix} = \pi \sum_{m_z} P_k(m_z) \int_{\theta^T}^{\theta^B} f_k^{(c)}(\theta) d\theta$$

$$= \pi \sum_{\tilde{m}} P_k(\tilde{m}) [F_k^{(c)}(\theta^B) - F_k^{(c)}(\theta^T)] \delta_{n_x m_x} \delta_{n_y m_y}, \tag{A6}$$

Where the summation over $\tilde{m}$ concerns only the unit cells existing inside the sphere of radius R^{cav} and centered in the i ion of the $\tilde{n}$ unit cell. It is noteworthy that θ^B and θ^T as well as **P** depend only on the third-component of $\tilde{m}$ (i.e., m_z). The primitive function, $F_k^{(c)}$, of the function $f_k^{(c)}$ is given by

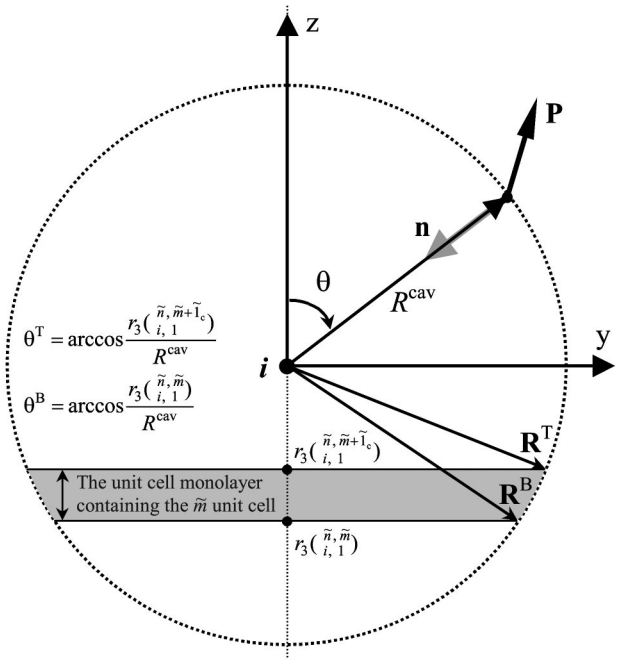

FIG. 7. Schematic of the Lorentz spherical cavity for c surface. $r_3\left(\begin{smallmatrix}\tilde{n},\tilde{m}\\ i,1\end{smallmatrix}\right)$ and $r_3\left(\begin{smallmatrix}\tilde{n},\tilde{m}+\tilde{1}_c\\ i,1\end{smallmatrix}\right)$ are, respectively, the bottom and top edge of the unit cell monolayer containing the $\tilde{m}$ unit cell. θ^B and θ^T are, respectively, the angles between z axis on one hand and the vectors $\mathbf{R}^B$ and $\mathbf{R}^T$ on the other hand. The center i coincides with the i-ion of the $\tilde{n}$ unit cell.

$$F_k^{(c)}(\theta) = \begin{cases} F_1^{(c)}(\theta) = -(\sin^2\theta\cos\theta + 2/3\cos^3\theta) \\ F_2^{(c)}(\theta) = -(\sin^2\theta\cos\theta + 2/3\cos^3\theta) \\ F_3^{(c)}(\theta) = -2/3\cos^3\theta, \end{cases} \tag{A7}$$

and

$$\theta^B = \arccos \frac{r_3\left(\begin{smallmatrix}\tilde{n},\tilde{m}\\ i,1\end{smallmatrix}\right)}{R^{cav}},$$

$$\theta^T = \arccos \frac{r_3\left(\begin{smallmatrix}\tilde{n},\tilde{m}+\tilde{1}_c\\ i,1\end{smallmatrix}\right)}{R^{cav}}. \tag{A8}$$

$(\tilde{m}+\tilde{1}_c)$ represents the unit cell having the coordinates (m_x, m_y, m_z+1) located on the top of the $\tilde{m}$ unit cell.

Finally the Lorentz cavity contribution to the local electric field in the k direction of the i ion located in the $\tilde{n}$ unit cell can be rearranged as:

$$E_k^{\mathrm{cav}}\begin{pmatrix}\tilde{n}\\ i\end{pmatrix}=\sum_{j=1}^{5}\sum_{\tilde{m}}\frac{\pi}{v(\tilde{m})}\left[F_k^{(c)}\left(\arccos\frac{r_3\begin{pmatrix}\tilde{n},\tilde{m}\\ i,1\end{pmatrix}}{R^{\mathrm{cav}}}\right)-F_k^{(c)}\left(\arccos\frac{r_3\begin{pmatrix}\tilde{n},\tilde{m}+\tilde{1}_c\\ i,1\end{pmatrix}}{R^{\mathrm{cav}}}\right)\right]\times\delta_{n_x m_x}\delta_{n_y m_y}p_k\begin{pmatrix}\tilde{n},\tilde{m}\\ i,j\end{pmatrix}. \tag{A9}$$

Note that **r**, **p**, and $v(\tilde{m})$ have been defined in Sec. II B.

APPENDIX B: CONNECTION BETWEEN THE ELECTRONIC POLARIZABILITIES AND THE EFFECTIVE ELECTRONIC POLARIZABILITIES

A three-dimensional Taylor series expansion of $p_k^{\mathrm{e}}(\mathbf{E}^{\mathrm{loc}})$ around the point $\mathbf{E}^{\mathrm{loc}}=\mathbf{E}^{\mathrm{spn}}$ ($\mathbf{E}^{\mathrm{spn}}$ is the local electric field in the spontaneous state) defines the α_{kl} element of the first-order electronic polarizability tensor, the $\beta_{kll'}$ element of the second-order electronic polarizability tensor, and the $\gamma_{kll'l''}$ element of the third-order electronic polarizability tensor as follows:[12]

$$p_k^{\mathrm{e}}=p_k^{\mathrm{e}}|_{\mathbf{E}^{\mathrm{loc}}=\mathbf{E}^{\mathrm{spn}}}+\sum_{l=1}^{3}\alpha_{kl}[E_l^{\mathrm{loc}}-E_l^{\mathrm{spn}}]+\frac{1}{2}\sum_{l=1}^{3}\sum_{l'=1}^{3}\beta_{kll'}[E_l^{\mathrm{loc}}-E_l^{\mathrm{spn}}][E_{l'}^{\mathrm{loc}}-E_{l'}^{\mathrm{spn}}]+\frac{1}{6}\sum_{l=1}^{3}\sum_{l'=1}^{3}\sum_{l''=1}^{3}\gamma_{kll'l''}[E_l^{\mathrm{loc}}-E_l^{\mathrm{spn}}][E_{l'}^{\mathrm{loc}}-E_{l'}^{\mathrm{spn}}]\times[E_{l''}^{\mathrm{loc}}-E_{l''}^{\mathrm{spn}}], \tag{B1}$$

$$\alpha_{kl}=\left.\frac{\partial p_k^{\mathrm{e}}}{\partial E_l^{\mathrm{loc}}}\right|_{\mathbf{E}^{\mathrm{loc}}=\mathbf{E}^{\mathrm{spn}}}, \tag{B2}$$

$$\beta_{kll'}=\left.\frac{\partial^2 p_k^{\mathrm{e}}}{\partial E_l^{\mathrm{loc}}\,\partial E_{l'}^{\mathrm{loc}}}\right|_{\mathbf{E}^{\mathrm{loc}}=\mathbf{E}^{\mathrm{spn}}}, \tag{B3}$$

$$\gamma_{kll'l''}=\left.\frac{\partial^3 p_k^{\mathrm{e}}}{\partial E_l^{\mathrm{loc}}\,\partial E_{l'}^{\mathrm{loc}}\,\partial E_{l''}^{\mathrm{loc}}}\right|_{\mathbf{E}^{\mathrm{loc}}=\mathbf{E}^{\mathrm{spn}}}, \tag{B4}$$

and

$$p_k^{\mathrm{e}}|_{\mathbf{E}^{\mathrm{loc}}=\mathbf{E}^{\mathrm{spn}}}=\sum_{l=1}^{3}\alpha_{kl}E_l^{\mathrm{spn}}-\frac{1}{2}\sum_{l=1}^{3}\sum_{l'=1}^{3}\beta_{kll'}E_l^{\mathrm{spn}}E_{l'}^{\mathrm{spn}}+\frac{1}{6}\sum_{l=1}^{3}\sum_{l'=1}^{3}\sum_{l''=1}^{3}\gamma_{kll'l''}E_l^{\mathrm{spn}}E_{l'}^{\mathrm{spn}}E_{l''}^{\mathrm{spn}}. \tag{B5}$$

The last equation is deduced from Eq. (B1) by taking into consideration that $p_k^{\mathrm{e}}|_{\mathbf{E}^{\mathrm{loc}}=0}=0$.

Equation (B1) can be rearranged as

$$p_k^{\mathrm{e}}=\sum_{l=1}^{3}\alpha_{kl}^{\mathrm{eff}}E_l^{\mathrm{loc}}+\frac{1}{2}\sum_{l=1}^{3}\sum_{l'=1}^{3}\beta_{kll'}^{\mathrm{eff}}E_l^{\mathrm{loc}}E_{l'}^{\mathrm{loc}}+\frac{1}{6}\sum_{l=1}^{3}\sum_{l'=1}^{3}\sum_{l''=1}^{3}\gamma_{kll'l''}^{\mathrm{eff}}E_l^{\mathrm{loc}}E_{l'}^{\mathrm{loc}}E_{l''}^{\mathrm{loc}}, \tag{B6}$$

where

$$\alpha_{kl}^{\mathrm{eff}}=\alpha_{kl}-\sum_{l'=1}^{3}\beta_{kll'}E_{l'}^{\mathrm{spn}}+\frac{1}{2}\times\sum_{l'=1}^{3}\sum_{l''=1}^{3}\gamma_{kll'l''}E_{l'}^{\mathrm{spn}}E_{l''}^{\mathrm{spn}}, \tag{B7}$$

$$\beta_{kll'}^{\mathrm{eff}}=\beta_{kll'}-\sum_{l''=1}^{3}\gamma_{kll'l''}E_{l''}^{\mathrm{spn}}, \tag{B8}$$

$$\gamma_{kll'l''}^{\mathrm{eff}}=\gamma_{kll'l''}. \tag{B9}$$

$\tilde{\alpha}^{\mathrm{eff}}$, $\tilde{\beta}^{\mathrm{eff}}$, and $\tilde{\gamma}^{\mathrm{eff}}$ are, respectively, the first-, second-, and third- order *effective* electronic polarizability tensors.

*Corresponding author: eng@iapp.de

[1] S. V. Kalinin and D. A. Bonnell, Phys. Rev. B **63**, 125411 (2001).
[2] L. Xuan, S. Pan, Z. Chen, R. Wang, W. Shi, and C. Li, Appl. Phys. Lett. **73**, 2896 (1998).
[3] T. Zhao, F. Chen, H. Lu, G. Yang, and Z. Chen, J. Appl. Phys. **87**, 7442 (2000).
[4] Y. Yoneda, T. Okabe, K. Sakaue, and H. Terauchi, J. Appl. Phys. **83**, 2458 (1998).
[5] Y. Yoneda, K. Sakaue, and H. Terauchi, J. Phys.: Condens. Matter **13**, 9575 (2001).
[6] J. Junquera and P. Ghosez, Nature (London) **422**, 506 (2003).
[7] H. Chaib, D. Khatib, and W. Kinase, Mol. Cryst. Liq. Cryst. Sci. Technol., Sect. B: Nonlinear Opt. **23**, 97 (2000).
[8] H. Chaib, A. Toumanari, D. Khatib, and W. Kinase, Ferroelectrics **234**, 61 (1999).
[9] H. Chaib, D. Khatib, A. Toumanari, and W. Kinase, J. Phys.: Condens. Matter **12**, 2317 (2000).
[10] H. Chaib, T. Otto, and L. M. Eng, Phys. Rev. B **67**, 174109 (2003).
[11] H. Chaib, T. Otto, and L. M. Eng, Phys. Status Solidi B **23**, 250 (2002); H. Chaib, F. Schlaphof, T. Otto, and L. M. Eng, J. Phys.: Condens. Matter **15**, 8927 (2003).
[12] S. P. A. Sauer, J. Phys. B **30**, 3773 (1997).
[13] J. C. Slater, Phys. Rev. **36**, 57 (1930).

[14] C. Kittel, *Introduction to Solid State Physics* (Wiley, New York, 1996).
[15] A. Yariv and P. Yeh, *Optical Waves in Crystals* (Wiley-Interscience, New York, 1984); Y. Sirotine and M. Chaskolskaia, *Fondements de la Physique des Cristaux* (MIR, Moscow, 1984).
[16] A. Toumanari, Ph.D. thesis, University of Agadir, Morocco, 1999.
[17] K. Nakamura and W. Kinase, J. Phys. Soc. Jpn. **61**, 2114 (1992).
[18] K. Nakamura and W. Kinase, J. Phys. Soc. Jpn. **61**, 4596 (1992).
[19] R. S. Cudney, J. Fousek, M. Zgonik, and P. Günter, Appl. Phys. Lett. **63**, 3399 (1993).
[20] A. R. Johnston and J. M. Weingart, J. Opt. Soc. Am. **55**, 828 (1965).
[21] J. D. Freire and R. S. Katiyar, Phys. Rev. B **37**, 2074 (1988).
[22] F. Gervais, P. Simon, P. Echegut, and B. Glas, Jpn. J. Appl. Phys., Part 1 **24**, 649 (1985).
[23] H. Pinto and A. Stashans, Phys. Rev. B **65**, 134304 (2002).
[24] Y. Kuroiwa, S. Aoyagi, A. Sawada, J. Harada, E. Nishibori, M. Takata, and M. Sakata, Phys. Rev. Lett. **87**, 217601 (2001).
[25] M. Born and K. Huang, *Dynamical Theory of Crystal Lattices* (Oxford University Press, Oxford, 1968).
[26] M. D. Fontana, G. Métrat, J. L. Servoin, and F. Gervais, J. Phys. C **16**, 483 (1984).
[27] R. Resta, M. Posternak, and A. Baldereschi, Phys. Rev. Lett. **70**, 1010 (1993).
[28] W. Zhong, R. D. King-Smith, and D. Vanderbilt, Phys. Rev. Lett. **72**, 3618 (1994).
[29] P. Ghosez and X. Gonze, J. Phys.: Condens. Matter **12**, 9179 (2000).
[30] J. D. Axe, Phys. Rev. **157**, 429 (1967).
[31] S. Tinte, M. G. Stachitti, M. Sepliarsky, R. L. Migoni, and C. O. Rodriguez, J. Phys.: Condens. Matter **11**, 9679 (1999).
[32] P. Ghosez, X. Gonze, and J. P. Michenaud, Ferroelectrics **153**, 91 (1994).
[33] K. Ishikawa and T. Uemori, Phys. Rev. B **60**, 11 841 (1999).
[34] L. Baudry and J. Tournier, J. Appl. Phys. **90**, 1442 (2001).
[35] T. Lu and W. Cao, Phys. Rev. B **66**, 024102 (2002).
[36] S. Tinte and M. G. Stachiotti, Phys. Rev. B **64**, 235403 (2001).
[37] J. Schubert, O. Trithaveesak, A. Petraru, C. L. Jia, R. Uecker, P. Reiche, and D. G. Schlom, Appl. Phys. Lett. **82**, 3460 (2003).
[38] A. Petraru, J. Schubert, M. Schmid, and Ch. Buchal, Appl. Phys. Lett. **81**, 1375 (2002).